A Mechanism-Based Reaction-Diffusion Model for Accelerated Discovery of Thermoset Resins Frontally Polymerized by Olefin Metathesis

Donald Bistri,[*,†,‡] Ignacio Arretche,[‡] Jacob J. Lessard,[¶,‡] Michael Zakoworotny,[†] Sagar Vyas,[†] Laurence Rongy,[§] Rafael Gómez-Bombarelli,[‖] Jeffrey S. Moore,[*,¶,‡] and Philippe Geubelle[*,†,‡]

†*Department of Aerospace Engineering, University of Illinois Urbana-Champaign, Urbana, IL, USA*

‡*Beckman Institute for Advanced Science and Technology, University of Illinois Urbana-Champaign, Urbana, IL, USA*

¶*Department of Chemistry, University of Illinois Urbana-Champaign, Urbana, IL, USA*

§*Nonlinear Physical Chemistry Unit, Faculté des Sciences, Université libre de Bruxelles, Brussels, Belgium*

‖*Department of Materials Science and Engineering, Massachusetts Institute of Technology, Cambridge, MA, USA*

E-mail: dbistri2@illinois.edu; jsmoore@illinois.edu; geubelle@illinois.edu

Abstract

Frontal ring-opening metathesis polymerization (FROMP) involves a self-perpetuating exothermic reaction, which enables the rapid and energy-efficient manufacturing of thermoset polymers and composites. Current state-of-the-art reaction-diffusion FROMP

models rely on a phenomenological description of the olefin metathesis kinetics, limiting their ability to model the governing thermo-chemical FROMP processes. Furthermore, the existing models are unable to predict the variations in FROMP kinetics with changes in the resin composition and as a result are of limited utility towards accelerated discovery of new resin formulations. In this manuscript, we formulate a chemically meaningful model grounded in the established mechanism of ring-opening metathesis polymerization (ROMP). Our study aims to validate the hypothesis that the ROMP mechanism, applicable to monomer-initiator solutions below 100°C, remains valid under the non-ideal conditions encountered in FROMP, including ambient to >200°C temperatures, sharp temperature gradients, and neat monomer environments. Through extensive simulations, we demonstrate that our mechanism-based model accurately predicts FROMP behavior across various resin compositions, including polymerization front velocities and thermal characteristics (e.g., T_{max}). Additionally, we introduce a semi-inverse workflow that predicts FROMP behavior from a single experimental data point. Notably, the physiochemical parameters utilized in our model can be obtained through DFT calculations and minimal experiments, highlighting the model's potential for rapid screening of new FROMP chemistries in pursuit of thermoset polymers with superior thermo-chemo-mechanical properties.

Introduction

Frontal polymerization (FP) is a self-sustaining reaction initiated by an energetic stimulus – thermal, chemical, or photo – which ignites a localized reaction front.[1] This process is characterized by the exothermic nature of the polymerization reaction as heat released from the unreacted monomer near the front raises the temperature locally. Crucially, the rise in temperature stems from the balance between the rate at which heat is released and the rate at which heat diffuses through the sample and is lost to the surroundings. With sufficient temperature rise, the polymerization front continues to propagate through the unreacted monomer phase until all reactants are consumed or significant heat loss stalls the reaction. Due to their self-sustaining nature, FP-curing routes have become a cost-effective and environmentally friendly alternative to the traditional, more resource-intensive manufacturing processes.[1–3] This advancement has spurred their versatile application in the efficient production of high-performance polymers, thermosets, composites, and hydrogels.[4–7]

Among the various polymerization methods, such as radical,[8–10] ionic,[11–13] and addition-type,[5] frontal ring-opening metathesis polymerization (FROMP) stands out significantly. FROMP utilizes well-defined initiator complexes, whose chemistry can be intentionally manipulated to fine-tune every step of the reaction, from inhibition, initiation, propagation, and termination. The capability to precisely control the reaction parameters enhances FROMP's attractiveness as it enables one to vary microscopic features such as heat release rate to in turn influence macroscopic features like front instabilities, front velocity, and resin storage time (i.e., pot life). The successful application of FROMP critically depends on the ability to balance rapid front progression with the risk of premature bulk polymerization at or near ambient temperatures.[14,15] Thus, synergistic experimental and computational efforts are crucial to accelerate the development and optimization of FROMP systems in light of the vast chemical design space.

Computationally, conventional FROMP models consist of a set of reaction–diffusion partial differential equations that govern the polymerization kinetics in terms of two gov-

erning field variables, the degree of cure, $\alpha(x,t)$ and the temperature, $T(x,t)$,

$$\begin{cases} \kappa \frac{\partial^2 T(x,t)}{\partial x^2} + \rho H_r \frac{\partial \alpha(x,t)}{\partial t} = \rho C_p \frac{\partial T(x,t)}{\partial t} \\ \frac{\partial \alpha(x,t)}{\partial t} = f(\alpha, T) = A \exp\Big(- \frac{E_a}{RT} \Big) g(\alpha). \end{cases}$$

Here, κ $[\frac{\mathrm{W}}{\mathrm{m \cdot K}}]$, C_p $[\frac{\mathrm{J}}{\mathrm{kg \cdot K}}]$, ρ $[\frac{\mathrm{kg}}{\mathrm{m}^3}]$, respectively denote the thermal conductivity, specific heat capacity, and density of the resin, while H_r $[\frac{\mathrm{J}}{\mathrm{kg}}]$, the total enthalpy of the polymerization reaction. Moreover, to describe the temperature dependent reaction kinetics, an Arrhenius equation is typically employed with A denoting a pre-exponential rate constant, E_a, the activation energy, and R, the universal gas constant. Lastly, as shown in Fig. 1(a), $g(\alpha)$ denotes an empirical reaction model.

While informative,[16–23] the existing computational FROMP models are phenomenological in their description of FP-kinetics, with cure kinetics parameters $\{A, E_a, g(\alpha)\}$ extracted from thermal analysis by differential scanning calorimetry (DSC) performed at different heating rates $\Big($c.f. Fig.1(a)$\Big)$.[19,24,25] Compounding to this, the standard DSC heating rates vary between $2-20^0$C/min, making the interface between experiments and computational models costly ($\approx$ 5 hours/resin formulation), while significantly undermining the localized FROMP rapid heating rates.

The existing literature has successfully established the mechanism of olefin metathesis for Grubbs' catalysts under meticulously controlled reaction conditions $\Big($i.e., low temperatures, (semi)dilute concentrations$\Big)$.[26–28] However, the conditions employed in these studies are significantly different than those encountered in FROMP. Understanding the kinetics of olefin metathesis beyond such "ideal" conditions (i.e., neat monomer at elevated temperatures) is scantly explored. Parameterized to DSC data, state-of-the-art empirical FROMP models are limited in their capacity to describe the underlying thermo-chemical processes governing the different FROMP reaction steps. Moreover, the restrictive one-way transfer of FROMP information from experiments to simulations, $\Big($c.f. Fig. 1(a)$\Big)$ limits the utility of conventional models for rapid screening of new resin formulations and accelerated material discovery. These limitations motivate the need for a mechanism-based,[9,29] chemically predictive model in concert with a closed-loop integration between experiments and simulations to facilitate the efficient nav-

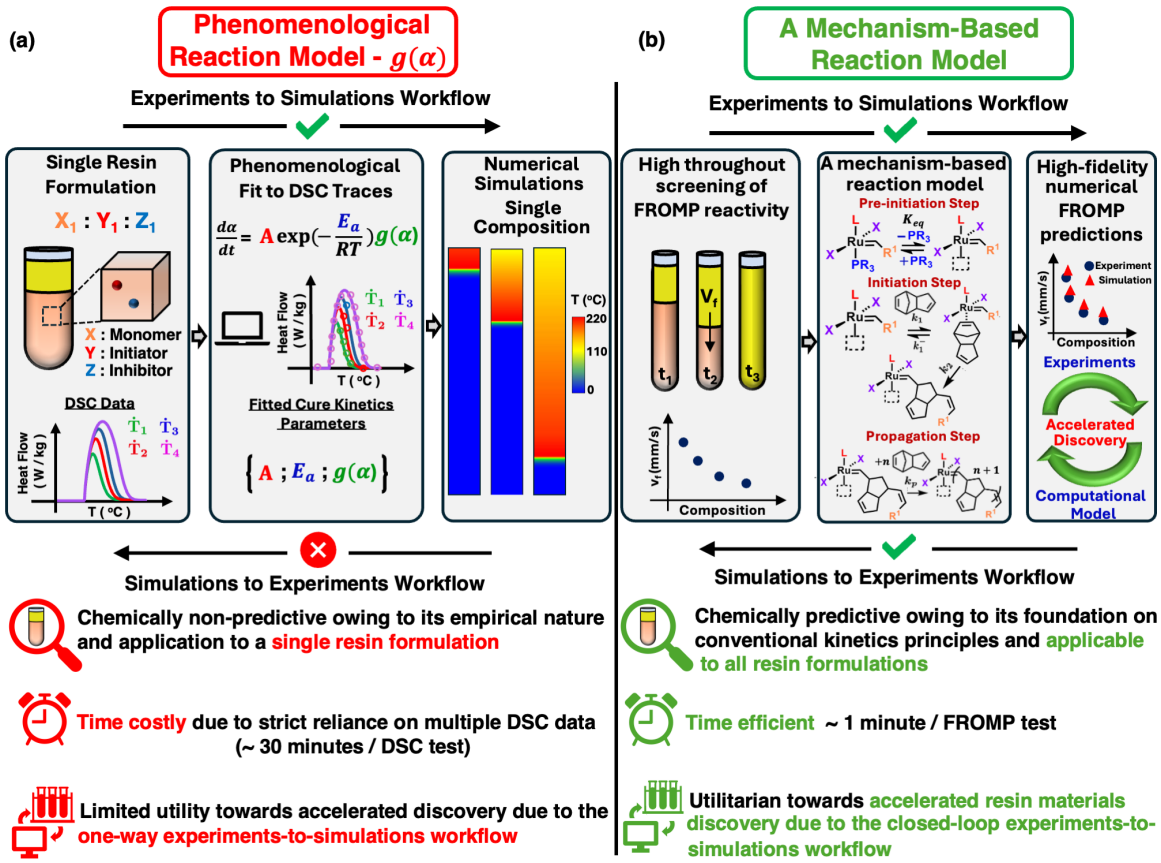

Figure 1: (a) Current state-of-the-art phenomenological FROMP reaction models, illustrating the one-way bypass of information from experimental DSC tests to empirical continuum level models. Owing to their strict reliance on DSC data, the existing models are limited in chemical predictability, time costly, and inefficient towards accelerated discovery of new resin formulations. (b) A mechanism-based reaction-diffusion model for systematic description of reaction kinetics associated with each FROMP step (inhibition, initiation, propagation). Constructed upon the conventional kinetics principles and chemically predictive in nature, the model establishes a rapid closed-loop communication between experiments and computational models to enable for the fast-screening of new resin formulations.

igation of the vast chemical design and parametric space.

To this end, we formulate a novel reaction-diffusion model, which systematically describes the FROMP mechanism through a three-step route (c.f. Fig. 1(b)). Constructed upon the conventional kinetics principles, the framework presented herein tests the Occam's razor hypothesis that adoption of the standard kinetics principles and physiochemical parameters established for ring-opening metathesis polymerization (ROMP) under ideal conditions can simultaneously capture FROMP attributes at elevated temperatures in neat

monomers. Validation of this hypothesis is not only of fundamental interest, but would additionally enable the computational screening of new chemical initiators and inhibitors for FROMP using computed activation energies and reaction thermodynamics. The proposed framework is grounded on a mechanism-based description of FROMP kinetics and systematically models the three steps outlined in Fig. 1(b), including the:

1. *Inhibition* step, which thermally gates the reactivity of the dormant inhibitor-bound ruthenium initiator by dissociation of the coordinated phosphine ligand prior to entry in the ring-opening olefin metathesis cycle.

2. *Initiation* step, which involves the 14-electron ruthenium initiator coordinating a strained olefin monomer to first form a metallacyclobutane by a [2+2] cycloaddition with the monomer, followed by a [2+2] ring-opening cycloreversion. This process is accompanied by heat release owing to the strained nature of the cyclic olefin and is irreversible for highly strained norbornene olefinic monomers.

3. *Propagation* step, which involves the sequential reaction of the initiated species with more olefin monomers (same mechanism as the initiation step) in a chain-growth polymerization process, which continues until the reaction stalls or all the monomer is consumed.

Through the proposed mechanism-based reaction model, we importantly demonstrate that the systematic adoption of conventional ROMP kinetics principles — including a temperature-dependent activation step – effectively applies to the non-ideal FROMP conditions (i.e., neat monomers at elevated temperatures) and can enable for high-fidelity predictions of macroscopic FROMP observables (e.g. front velocity). Importantly, we note that these macroscopic FROMP observables (e.g., front velocity) are experimentally acquired within seconds via high throughput FROMP reactivity screening across many resin formulations, Fig. 1(b), eliminating the reliance on time-costly DSC tests. Consistent with experiments, we demonstrate the capacity of the model to predict FROMP reactivity with variation in the monomer:initiator:inhibitor composition for a dicyclopentadiene – Grubbs'

2^{nd} generation initiator – tributyl phosphite (DCPD:G2:TBP) system recently reported by Lessard et al.[30] Apart from variations in the resin chemical composition, the change in polymerization front speed with process conditions, respectively the initial resin temperature, is additionally simulated for the same DCPD:G2:TBP system and shown to be in good quantitative agreement with in-house experiments.

Lastly, we demonstrate the utility of the model towards rapid screening of different resin chemistries (i.e., monomer/initiator/inhibitor). Concretely, we develop a "semi-inverse" workflow – detailed at the end of the manuscript – and simulate FROMP reactivity for a separate resin formulation, which includes a distinct ruthenium complex to the previous G2 initiator, respectively a M207 Grubbs' initiator. In doing so, we demonstrate consistent predictions in FROMP reactivity with in-house experiments and critically establish a closed-loop integration between experiments and simulations $\Big($c.f. Fig. 1 (b)$\Big)$, a missing link in the conventional empirical FROMP models.

All in all, the proposed framework presents a time-efficient, chemically predictive computational tool which – jointly with experiments – can accelerate the identification of optimal resin chemistries for the efficient manufacturing of thermoset polymers with superior engineering properties.

Results and Discussion

Formulation of a three-step reaction-diffusion FROMP model

We describe herein a systematic formulation of a three-step reaction-diffusion model for ruthenium-initiated FROMP. Ruthenium-based complexes have been extensively used in organic and polymer chemistry due to their high reactivity with olefinic substrates in the presence of most common functional groups.[31] Without loss of generality, we consider a class of ruthenium complexes with the general formula $L(PR_3)(X)_2Ru{=}CHR^1$ as schematically shown in Fig. 2(a).[†] Here, $\{L, R, X, R^1\}$ represent different substituents, whose selection

[†]As the developed mechanism-based framework is general in nature and can be equivalently applied across a variety of ruthenium-initiated FROMP systems, we present the formulation in its general form, prior to specializing for resin formulations of choice in subsequent sections.

modulates the kinetics of both the initiation and propagation steps as detailed in Sanford et al.[31] For convenience, Fig. 2(b-c) illustrate a set of typical ruthenium complexes obtained for different substituents.

Prior to entry of the ruthenium complex into the olefin metathesis cycle, dissociation of the inhibitory phosphine ligand (i.e., PR_3) must occur to unveil the reactivity of the dormant 16-electron ruthenium initiator, (**II**). This step, known as the pre-initiation or the inhibition step, is schematically shown in Fig. 2(d). At room temperature, the phosphine ligand, PR_3, is thermodynamically favored to coordinate to the metal center of the ruthenium complex, which inhibits polymerization. At high temperature, increased entropic effects favor phosphine dissociation, leading to formation of an active ruthenium complex shown as (**AI**) in Fig. 2(d). Modeling the dissociation of the inhibitory phosphine ligand is critical as it allows for entry of the ruthenium initiator into the olefin metathesis catalytic cycle, directly affecting the kinetics of the subsequent initiation and propagation steps.

To numerically resolve the temperature

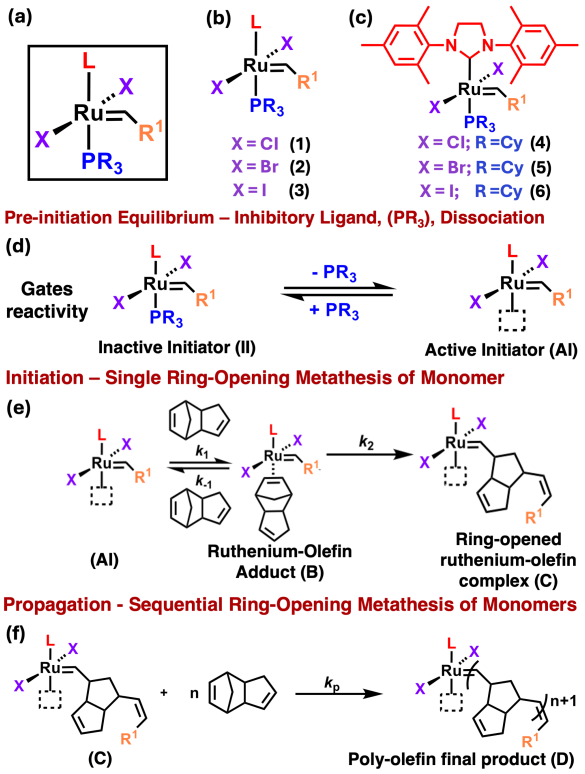

Figure 2: (a) Chemical representation of ruthenium complexes with the general formula $L(PR_3)(X)_2Ru{=}CHR^1$. (b–c) Representative ruthenium complexes obtained for different {L, R, X, R^1} substituents. (d) Inhibition equilibrium step, illustrating the dissociation of the inhibitory ligand, PR_3, from the dormant ruthenium initiator to form an active complex. (e) Initiation step, during which a ring-opening olefin metathesis reaction initiated by the active ruthenium complex instigates, resulting in the formation of a ruthenium-olefin complex followed by heat release. (f) Propagation step, illustrating the sequential addition of olefin monomers to the initiated ruthenium-olefin complex to produce a solid polymer material.

dependent evolution in concentration of the active ruthenium initiator, (**AI**), a fast-equilibrium assumption is employed. As a result, the pre-initiation step which gates reactivity

can be characterized by its equilibrium constant, K_{eq}. By virtue of the Van't Hoff relationship, the temperature-dependent evolution of the equilibrium constant, K_{eq}, can be related to the standard enthalpy, ΔH^o, and standard entropy, ΔS^o, of the phosphine dissociation reaction, yielding

$$K_{\text{eq}} = \exp\Big(- \frac{\Delta H^o}{RT} + \frac{\Delta S^o}{R} \Big) \qquad (1)$$

Furthermore, on the basis of the law of mass action, the dissociative inhibition equilibrium can be further expressed as the product of the reactants' concentrations,

$$K_{\text{eq}} = \frac{[\mathbf{AI}][\mathbf{PR}_3]}{[\mathbf{II}]} \qquad (2)$$

Here, [**II**] denotes the concentration of the dormant inhibitor-bound ruthenium complex, [$\mathbf{PR}_3$], the concentration of the dissociated inhibitor, and [**AI**], the concentration of the active ruthenium complex (i.e., active initiator).

Jointly, eqns. (1) and (2) describe the temperature-dependent evolution of the concentration of reaction species participating in the inhibition step. Establishing such association is critical for numerically resolving the temperature-dependent evolution in concentration of the active initiator, [**AI**], the latter directly entering the metathesis catalytic cycle for FROMP.

Towards this goal and starting with a $\Big([\mathbf{II}_0],\ [\mathbf{AI}_0],[\mathbf{PR}_3^0]\ \Big)$ composition, let [$\mathbf{AI}^+$] denote the amount of the active ruthenium complex produced during the phosphine dissociation reaction. Combining eqns. (1) – (2) and performing a series of algebraic manipulations, it can be shown that the temperature dependent amount of the generated active initiator, [$\mathbf{AI}^+$], evolves as a function of the starting composition [†] through the following relationship,

$$[\mathbf{AI}^+] = -\frac{[\mathbf{AI}_0] + [\mathbf{PR}_3^0] + K_{\text{eq}}}{2} + \ldots + \frac{1}{2}\sqrt{\Big([\mathbf{AI}_0] + [\mathbf{PR}_3^0] + K_{\text{eq}}\Big)^2 \ldots - 4\Big([\mathbf{AI}_0][\mathbf{PR}_3^0] - K_{\text{eq}}[\mathbf{II}_0]\Big)} \qquad (3)$$

Eqn. 3 importantly governs the temperature-dependent activation of the ruthenium initiator prior to entry in the metathesis catalytic

[†]Numerically, we update the starting composition $\Big([\mathbf{II}_0],\ [\mathbf{AI}_0],[\mathbf{PR}_3^0]\Big)$ at each solution step of the model to accordingly account for the activation of a [$\mathbf{AI}^+$] amount of the dormant initiator from the previous inhibition solution step.

cycle for FROMP.

We transition next to describing the initiation step kinetics. During this step, the active ruthenium complex, (**AI**), binds to the strained olefinic monomer substrate first to form a four-coordinate intermediate ruthenium-olefin adduct, (**B**) as shown in Fig. 2(e). The ruthenium-olefin adduct undergoes initiation by [2+2] cycloaddition and subsequently cycloreversion, resulting in the formation of a ruthenium-olefin complex with a single ring-opened monomer attachment, (**C**). This process is accompanied by ring-strain relaxation in the latter, contributing to the heat release.

For later use and nomenclature convenience, we introduce $[\mathbf{M}_0]$ to denote the initial concentration of the olefinic monomer in the system, while $[\mathbf{M}]$, the respective concentration of the olefinic monomer consumed through polymerization. The degree of cure, α, can then be evaluated as,

$$\alpha = \frac{[\mathbf{M}]}{[\mathbf{M}_0]} \in [0, 1] \tag{4}$$

Here, a state of $\alpha = 0$ represents the uncured liquid monomer resin, while $\alpha = 1$, a state of complete conversion of the liquid resin into a solid polymer. All intermediary α–states denote a partially-cured resin.

Application of the steady-state approximation to the four-coordinate ruthenium-olefin adduct, that is $\frac{d[\mathbf{B}]}{dt} = 0$, in conjunction with the rate law for first-order reactions yields the following equality,

$$k_1[\mathbf{AI}][\mathbf{M}_0 - \mathbf{M}] = (k_{-1} + k_2)[\mathbf{B}] \tag{5}$$

Solving for $[\mathbf{B}]$ from eqn. 5 gives,

$$[\mathbf{B}] = \frac{k_1}{k_{-1} + k_2}[\mathbf{AI}][\mathbf{M}_0 - \mathbf{M}] \tag{6}$$

By virtue of the rate law and making use of eqn. 6, the rate at which the ruthenium-olefin complex, (**C**), forms can be computed as follows,

$$\frac{d[\mathbf{C}]}{dt} = k_2[\mathbf{B}] = \bar{k}_i[\mathbf{AI}][\mathbf{M}_0 - \mathbf{M}]^{\dagger} \tag{7}$$

Here, $\bar{k}_i = \frac{k_1 k_2}{k_1^- + k_2}$ denotes an effective initiation rate constant in units of $[\frac{\text{liter}}{\text{mol·s}}]$. Alter-

[†]We remark here that $[\mathbf{AI}]$ denotes the net concentration of the active initiator during the current initiation kinetics solution step. We continuously update $[\mathbf{AI}]$ in our numerical implementation of the model to account for the combined (i) production of the active initiator, $[\mathbf{AI}+]$ during the current pre-initiation solution step and (ii) consumption of the active initiator by an amount of $\delta[\mathbf{C}]$ during the initiation reaction from the prior solution step.

natively, factoring out $[\mathbf{M}_0]$, one can additionally introduce an effective concentration-dependent initiation rate constant, $\mathrm{k}_i^{eff} = \bar{k}_i[\mathbf{M}_0]$ with units of $[\frac{1}{s}]$. On this note, eqn. 7 can be rewritten as follows

$$\frac{d[\mathbf{C}]}{dt} = k_i^{eff}[\mathbf{AI}](1-\alpha) \tag{8}$$

As is standard, to describe the temperature dependence of the effective initiation reaction constant, k_i^{eff}, we append an Arrhenius-type kinetics to our formulation, such that $k_i^{eff} = A_i \cdot \exp\left(-\frac{E_a^i}{RT}\right)$. Here, A_i, denotes an effective initiation pre-exponential factor in units of $[\frac{1}{s}]$, while E_a^i, an effective initiation activation energy in units of $[\frac{\mathrm{J}}{\mathrm{mol}}]$.

Lastly, as evident from eqn. 8, we remark that the rate of formation of the ruthenium-olefin complex, $(\mathbf{C})$, is proportional to the concentration of the active initiator, $[\mathbf{AI}]$, reflecting the direct coupling between the inhibition and the initiation step in our mechanism-based model.

We transition next to describing the reaction kinetics associated with the propagation step. During this step, the ruthenium-olefin complex, $(\mathbf{C})$, sequentially reacts with n-olefin monomer units in a irreversible chain growth polymerization process, similar in mechanism to the initiation step. This results in the formation of a solid polymer material, Fig. 2(f). By virtue of the law of mass action and accounting for the one-at-a-time sequential coordination of the olefin monomers to the ruthenium-olefin complex, one can describe the rate of the olefin units conversion into a solid poly-olefin as follows

$$\frac{d[\mathbf{M}]}{dt} = k_p[\mathbf{C}][\mathbf{M}_0 - \mathbf{M}] \tag{9}$$

Here, k_p, denotes a propagation reaction constant in units of $[\frac{\mathrm{liter}}{\mathrm{mol}\cdot\mathrm{s}}]$. Similar to our earlier discussion on the initiation reaction kinetics, factoring out $[\mathbf{M}_0]$, one can introduce an effective concentration-dependent propagation rate constant, $k_p^{eff} = k_p[\mathbf{M}_0]$ in units of $[\frac{1}{s}]$. Rewriting eqn. 9 in terms of the degree of cure, α, then yields

$$[\mathbf{M}_0]\frac{d\alpha}{dt} = k_p^{eff}[\mathbf{C}](1-\alpha) \tag{10}$$

To describe the temperature dependence of the propagation rate constant, k_p^{eff}, we again append an Arrhenius-type kinetics to our formulation such that $k_p^{eff} = A_p \cdot \exp\left(-\frac{E_a^p}{RT}\right)$.

Here, A_p, denotes an effective propagation pre-exponential factor in units of $[\frac{1}{s}]$, while E_a^p, an effective propagation activation energy in units of $[\frac{\mathrm{J}}{\mathrm{mol}}]$.

Additionally, as evident from eqn. 10, we remark that the evolution in the degree of cure, α, is proportional to $[\mathbf{C}]$, highlighting the cascade coupling between the initiation and the propagation steps in our formulation. Upon full conversion of the monomer to a solid polymer, that is $\alpha = 1$, the propagation step concludes. We additionally remark that – as a first approximation to the model – an assumption of no termination step, cross-metathesis or catalyst decomposition is employed (c.f. Cooper et al.[32]).

As a last constituent to our three-step reaction-diffusion formulation, we discuss next the governing equation for temperature evolution with heat release during frontal polymerization of the liquid monomer resin. To describe both the time and spatial evolution of the temperature field, $T(x,t)$, we invoke the standard heat balance equation, such that

$$\kappa \frac{\partial^2 T(x,t)}{\partial x^2} + \rho H_r \frac{\partial \alpha(x,t)}{\partial t} = \rho C_p \frac{\partial T(x,t)}{\partial t} \tag{11}$$

Here, κ $[\frac{\mathrm{W}}{\mathrm{m}\cdot\mathrm{K}}]$, C_p $[\frac{\mathrm{J}}{\mathrm{kg}\cdot\mathrm{K}}]$, ρ $[\frac{\mathrm{kg}}{\mathrm{m}^3}]$, respectively denote the thermal conductivity, specific heat capacity, and density of the resin, while H_r $[\frac{\mathrm{J}}{\mathrm{kg}}]$, the total enthalpy of the polymerization reaction. The delicate balance of reaction rates, exothermicity, and efficient heat transport into the unpolymerized media is critical and determines both the propensity for the polymerization front to sustain itself in addition to characteristics of the latter (i.e., stable versus unstable propagation).

All in all, our three-step reaction-diffusion formulation can be summarized by the following set of equations for a total of four solution variables, $\Big([\mathbf{AI}^+(x,t)],\ [\mathbf{C}(x,t)], \alpha(x,t),\ T(x,t)\ \Big)$,

$$\begin{cases} [\mathbf{AI}^+] = -\dfrac{[\mathbf{AI}_0] + [\mathbf{PR}_3^0] + K_{\mathrm{eq}}}{2} + \ldots \\ \qquad + \dfrac{1}{2}\sqrt{\Big([\mathbf{AI}_0] + [\mathbf{PR}_3^0] + K_{\mathrm{eq}}\Big)^2 \ldots \\ \qquad - 4\Big([\mathbf{AI}_0][\mathbf{PR}_3^0] - K_{\mathrm{eq}}[\mathbf{II}_0]\Big)} & (1) \\ \frac{d[\mathbf{C}]}{dt} = k_i^{eff}[\mathbf{AI}](1-\alpha) & (2) \\ [\mathbf{M}_0]\frac{d\alpha}{dt} = k_p^{eff}[\mathbf{C}](1-\alpha) & (3) \\ \kappa \frac{\partial^2 T(x,t)}{\partial x^2} + \rho H_r \frac{\partial \alpha(x,t)}{\partial t} = \rho C_p \frac{\partial T(x,t)}{\partial t} & (4) \end{cases} \tag{12}$$

subjected to the hereinafter initial conditions, $[\mathbf{C}(x,0)] = [\mathbf{C}_0]$, $\alpha(x,0) = \alpha_0$, and $T(x,0) =$

T_0, for a starting $\left([\mathbf{M_0}], [\mathbf{II}_0], [\mathbf{PR}_3^0]\right)$ monomer-initiator-inhibitor composition. As is conventionally the case in the literature, these equations are supplemented with a thermal trigger applied as either a Dirichlet temperature, T_{trig}, or Neumann heat flux, $-\mathbf{q}\cdot\mathbf{n} = \tilde{q}$, boundary condition on one end of the simulation domain over a short time interval $[0, t_{\text{trig}}]$. Beyond this time interval, the thermal stimuli is removed to enable for self-sustained polymerization consistent with experiments.

We transition next to discussing a series of numerical simulations serving to highlight the capabilities of our framework in predicting FROMP kinetics with variation in both the monomer:initiator:inhibitor composition and chemical system identity. Throughout this process, we validate our numerical findings against published experimental data in the literature or in-house experiments.

On the role of monomer:initiator:inhibitor on dicyclopentadiene FROMP kinetics.

While FP-curing has been shown to be viable for a range of monomers including acrylates[33] and epoxies,[34] dicyclopentadiene (DCPD) has attracted much research attention owing to its engineering properties, including high reactivity, good strength to weight ratio, high flexibility and durability.[2] In particular, the ring-opening metathesis reaction of DCPD initiated and propagated by ruthenium alkylidenes containing N-heterocyclic carbene (NHC) ligands $\left(\text{i.e., Grubbs' } 2^{\text{nd}} \text{ generation initiator, c.f. Fig. 2(c)}\right)$ has been widely reported in the literature owing to the dramatically increased reactivity of the latter with olefinic substrates.[31,35] Nevertheless, such high reactivity comes at the expense of a reduced storage time due to background reactivity at room temperature depleting the amount of available initiator and monomer.

To temper background reactivity, while enabling FROMP to occur upon thermal activation, different catalytic inhibitors have been explored, including triphenylphosphine,[36] 4-dimethylaminopyridine[37] etc. These studies have reported sustained storage times of up to 10 minutes. Nevertheless, a longer storage time is desirable for processing purposes, requiring the liquid monomer solution to persist in excess of one hour.

Towards this goal, Robertson and co-workers demonstrated that introduction of an inhibitory alkyl phosphite ligand in a ruthenium-benzylidene Grubbs' 2nd generation complex, (**G2**), significantly suppresses room-temperature reactivity towards DCPD, while maintaining efficient reactivity at high temperatures.[38] Depending on the concentration of the dissolved tributyl phosphite (TBP) inhibitor in a DCPD/G2 (monomer/initiator) solution, the degree of control on both storage life and FROMP reactivity can be modulated. Fig. 3(a) illustrates a schematic of the DCPD/G2 solution (light orange) in which the TBP inhibitor is dissolved for controlled bulk reactivity. Moreover, Fig. 3(b) additionally illustrates the dissociation mechanism of the inhibitory ligand in the form of either (i) a tricyclohexylphosphine (PCy_3) ligand coordinated to the initial dormant Grubbs' 2nd generation initiator or (ii) a tributyl phosphite ligand, $P(OBu)_3$, initially dissolved in DCPD, which coordinates to the ruthenium alkylidene complex to form a latent precatalyst complex in situ.

Experimental investigations of the effect of variations in the monomer:initiator:inhibitor loading on the rate of frontal polymerization have only recently been reported. In particular, Lessard et al.[30] reported such a systematic experimental study on the DCPD:G2:TPB system illustrated in Fig. 3(a). Studies of this nature and their further supplementation with robust computational models are promising for the identification of novel frontally-polymerized thermosets.

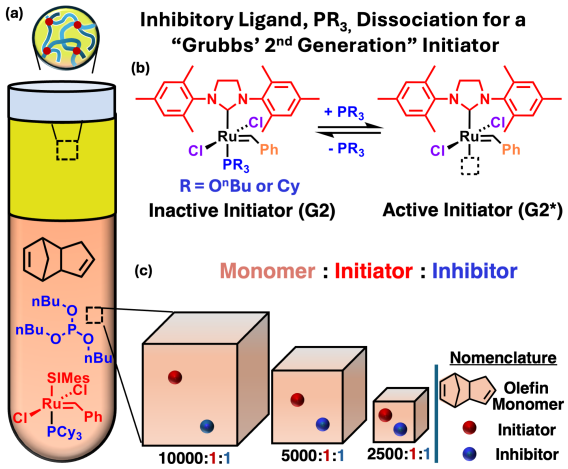

Figure 3: (a) Schematic illustration of a DCPD:G2:TBP liquid resin (light orange), mimicking the experimental setup by Lessard et al.[30] For convenience, the fully-polymerized resin is shown in yellow, distinctively demarcating the polymerization front. (b) Illustrates the inhibitory ligand, PR_3, dissociation for a Grubbs' 2nd generation initiator during the pre-initiation activation step. (c) Illustrates a representative volume element (RVE) for [2500 – 10000]:1:1 monomer:initiator:inhibitor resin compositions. From left to right, as the monomer-to-initiator loading ratio decreases, the molar concentrations of both the inhibitor and the initiator equally increase.

Using the newly-proposed mechanism-based FROMP model, we perform finite element simulations to numerically reproduce the experimentally reported variation in FROMP reactivity of a DCPD:G2:TBP system with (i) changes in the relative DCPD:G2 monomer to initiator loading, while fixing the inhibitor equivalence and (ii) changes in the TBP inhibitor loading, while preserving the DCDP:G2 monomer to initiator loading ratio fixed.

The fully-coupled system of equations outlined in eqn. 12 is numerically solved using the finite element method through development of a 1-D staggered solver discretized with continuous first-order Lagrange elements using the open-source FEniCS computing platform.[39] To numerically solve for the concentration degrees of freedom, $\Big([\mathbf{C}(x,t)],\, \alpha(x,t)\Big)$, an explicit Euler scheme with a sufficiently small time discretization for numerical accuracy is utilized. Upon casting eqn. $12_{(4)}$ into a linear variational problem, the partial differential equation governing heat diffusion is implicitly solved for the temperature field, $T(x,t)$, using an iterative conjugate-gradient Krylov solver.

A key challenge associated with FP modeling is the need to capture the sharp gradients in temperature and degree of cure present in the moving front. The ability to resolve such sharp gradients requires a highly-refined spatial discretization of the simulation domain. On this note, a uniform mesh with a sufficiently small element size ($dx = 1\,\mu$m for a simulation domain length, $L = 0.02\,$m) is employed for our meshing needs.

The fully-coupled system of equations is supplemented with the following initial conditions, $\alpha(x,0) = 0.01$, $[\mathbf{C}(x,0)] = 0$, $T(x,0) = 23^{\circ}$C for a starting $\Big([\mathbf{M}_0],\, [\mathbf{II}_0],\, [\mathbf{PR}_3^0]\Big)$ monomer:initiator:inhibitor composition. We numerically prescribe the initial resin composition to systematically replicate the experiments by Lessard et al.[30] In particular, we model FROMP reactivity for [500 - 10000]:1:x DCPD:G2:TBP resin formulations, with x denoting the inhibitor molar equivalents ranging from 0.25 – 1 $\Big($c.f. Fig. 3(c)$\Big)$. We refer the reader to Tab. S1 – S3 in the Supplementary Information (SI) for tabulated concentration data across the different resin compositions, $\Big([\mathbf{M}_0],\, [\mathbf{II}_0],\, [\mathbf{PR}_3^0]\Big)$ simulated in this work.

To initiate FROMP, we apply a trigger

Table 1: Physiochemical parameters for numerical simulation of FROMP reactivity in a DCPD:G2:TBP resin system

	Parameter	Value	Source
Heat Diffusion	κ	0.15 W/(m·K)	Vyas et al.[40]
	ρ	980 kg/m^3	Vyas et al.[40]
	C_p	1600 J/(kg·K)	Vyas et al.[40]
	H_r	381482 J/kg	Lessard et al.[30]
Reaction Kinetics	ΔH^o	26.1 kCal/mol	Adlhart and Chen[41]
	ΔS^o	57 Cal/(mol· K)	Adlhart and Chen[41] Lessard et al.[30]
	A_i^{eff}	1.1–2.25 $\cdot$ 10^{11} 1/s	Sanford et al.[31]
	A_p^{eff}	1.1–2.25 $\cdot$ 10^{13} 1/s	Fitted to Lessard et al.[30]
	E_p^{eff}	74000 J/mol	Kessler & White[24]
	E_i^{eff}	74000 J/mol	This work

temperature, $T_{\text{trig}} = T_{\max} = T_0 + \frac{Hr}{C_p}(1-\alpha_0)$, for a short period of time, $t \in [0, t_{\text{trig}}]$, at the left edge ($x = 0$). Past t = t_{trig}, the left boundary is insulated. Adiabatic conditions are imposed at $x = L$ throughout the simulation.

The relevant physiochemical parameters for our DCPD:G2:TBP system are tabulated in Tab. 1. While the mechanism-based nature of the framework allows virtually all material parameters to be found from the literature, (either experimentally or from ab-initio computations), the following remarks are made concerning the prescription of the effective initiation activation energy, E_i^{eff}, and the effective propagation pre-exponential constant, A_p^{eff},

(i) Motivated by the scarcity of the literature data, we assume from the start the effective initiation activation energy, E_i^{eff}, to be equal to the effective propagation activation energy, E_p^{eff}, reported in Kessler and White.[24]

(ii) With the initiation pre-exponential constant, A_i^{eff}, prescribed from Sanford et al.,[31] A_p^{eff} is computed through an iterative fitting process until a converging front velocity is achieved to the experiments by Lessard et al.[30] for a single DCPD:G2:TBP resin composition. FROMP reactivity for all the remaining DCPD:G2:TBP resin compositions is subsequently simulated and the numerical front ve-

locity predictions are compared against experiments.

Fig. 4 illustrates the numerical predictions in polymerization front velocity for [500 – 10000] :1:x DCPD:G2:TBP resin formulations using our mechanism-based FROMP model. From left to right, the inhibitor loading equivalence (i.e., x) is systematically varied from 0.25 – 1. To compare the performance of the mechanism-based model to conventional FROMP models built upon a phenomenological cure-kinetics formulation, $g(\alpha)$, Fig. 4(c) additionally includes FROMP reactivity predictions using the state-of-the-art empirical models[16,19,23] †. We refer the reader to Tab. S4 in the SI for tabulated numerical front velocities across the different resin compositions shown in Fig. 4.

Across the different inhibitor loadings (from left to right), we remark that the numerical front velocities using the mechanism-based model are in good quantitative agreement with the experiments by Lessard et al.[30] Remarkably, this finding supports our starting Oc-

†Empirical FROMP models have been primarily reported for x:1:1 DCPD:G2:TBP resin compositions. On this note, the comparison between the existing phenomenological FROMP model[16,19,23] and the newly-proposed mechanism-based model is only reported for these resin compositions.

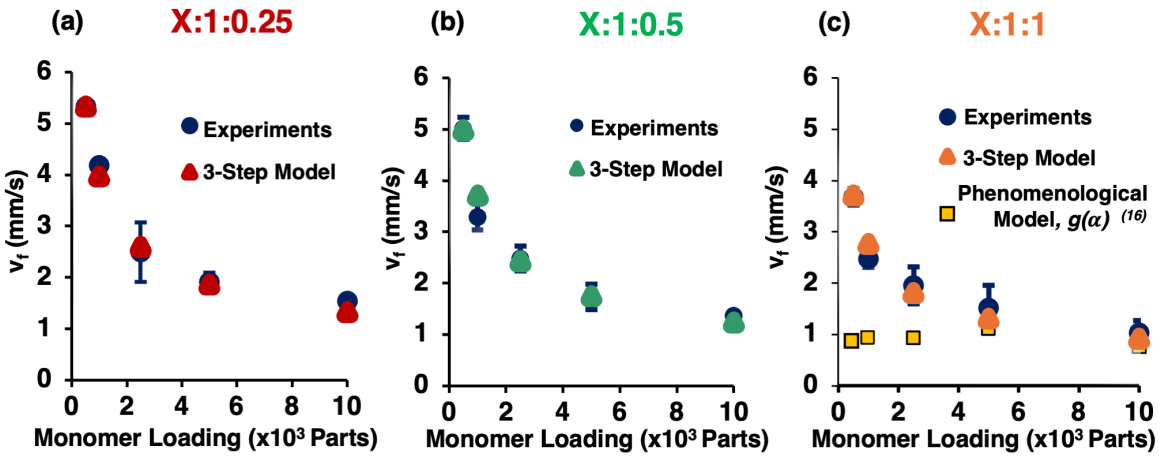

Figure 4: Comparison between numerical and experimental polymerization front velocities for a DCPD:G2:TBP system with a monomer-to-initiator loading ratio of [500-10000]:1, each coupled to an inhibitor molar equivalent of 0.25 (left), 0.5 (middle) and 1.0 (right). Across the three different TBP inhibitor loading ratios (left to right), the numerical front velocity predictions using the mechanism-based three-step model are in good quantitative agreement with the experiments by Lessard et al.[30] All simulations use identical physiochemical parameters (Table 1).

cam's razor hypothesis that the adoption of standard kinetics principles and associated physiochemical parameters established for ROMP under ideal conditions can simultaneously capture FROMP attributes at elevated temperatures. In great contrast, phenomenological models[16,19] are unable to numerically replicate the experimental variation in front velocity with the change in resin composition, predicting a constant front velocity across. This limitation stems from their strict parametrization to experimental DSC traces, the latter being unable to capture differences in cure kinetics across the different monomer:initiator:inhibitor resin compositions.

One further notices that the velocity of the polymerization front continuously increases as the monomer-to-initiator ratio decreases for a fixed inhibitor loading. As detailed in Lessard et al.,[30] a decrease in the monomer-to-initiator ratio (i.e., increase in the initiator and inhibitor concentration at fixed inhibitor equivalents) increases the amount of the Grubbs' 2nd generation initiator that can be activated $\left(\text{i.e., } [\mathbf{G2^*}] \text{ from Fig. 3(b)}\right)$ at elevated temperatures during the inhibition equilibrium step. This stems from decreased inhibition at elevated temperatures due to the entropically favored ligand dissociation. The proportional increase in the amount of initiator that can be activated, $\left(\text{i.e., } [\mathbf{G2^*}]\right)$, with decrease in the monomer-to-initiator loading ratio is illustrated in Fig. 5(a) for a representative [500–10000]:1:1 resin composition. In

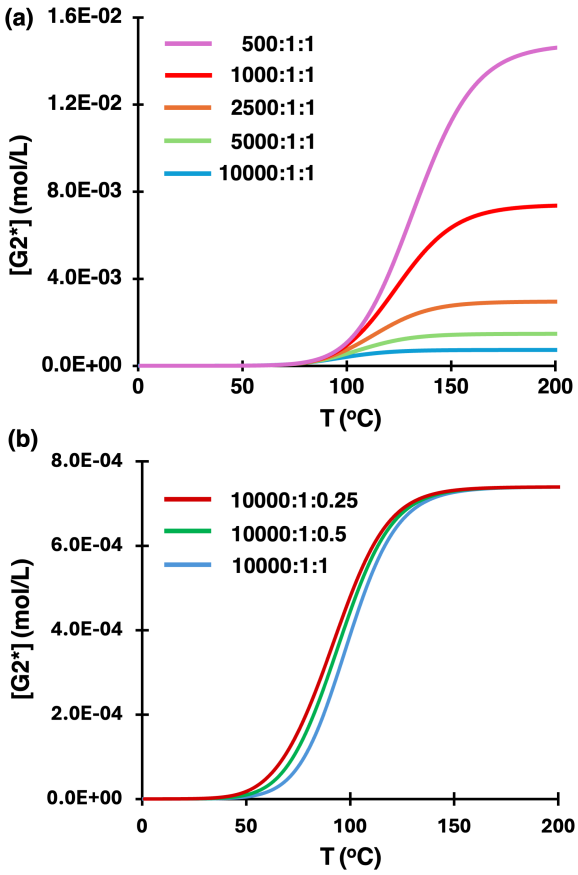

Figure 5: (a) Evolution in the concentration of active initiator, $[\mathbf{G2^*}]$ with temperature for (a) [500-10000]:1:1 and (b) 10000:1:x with $x \in \{0.25; 0.5; 1.0\}$ resin compositions.

light of eqns. $12_{(2-3)}$, this increase in concentration enhances both the initiation and the propagation reaction kinetics due to the cou-

pling between the different reaction steps in our mechanism-based model.

Fig. 6 additionally illustrates the variation in the polymerization front velocity with changes in the TBP inhibitor loading. Con-

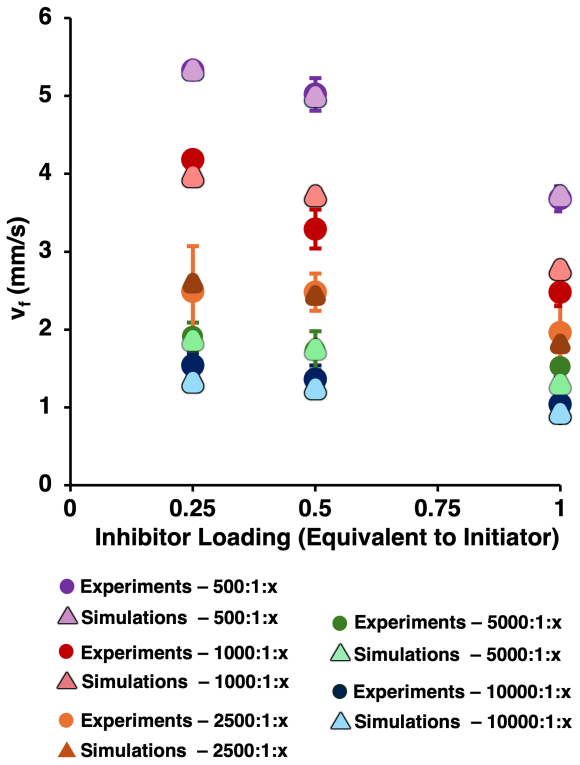

Figure 6: Variation in the simulated polymerization front velocity with change in the TBP inhibitor loading for a DCPD:G2 monomer-to-initiator ratio of [500-10000]:1. The simulated polymerization front velocities are in good quantitative agreement with the experiments by Lessard et al.[30] and illustrate the gradual decrease in front velocity with increase in the TBP inhibitor loading for a fixed monomer-to-initiator composition (left to right). All simulations use a consistent set of physiochemical parameters (Table 1).

sistent with the Occam's razor hypothesis and reports in the literature,[30,38] an increase in the TBP inhibitor loading for a fixed monomer-to-initiator ratio (left to right) retards the activation of the dormant G2 ruthenium initiator during the inhibition equilibrium step, slowing down FROMP kinetics overall. The delayed activation of the dormant Grubbs' 2nd generation initiator (rightward shift) is also graphically shown in Fig. 5(b) for a representative 10000:1:x resin composition.

We expand this study and additionally simulate the effect of the resin processing conditions, namely the initial resin temperature, T_0, on FROMP reactivity across different DCPD:G2:TPB resin compositions. Apart from the room temperature FROMP reactivity reported by Lessard et al.,[30] we perform experiments for model validation at an elevated resin temperature, $T_0 = 35^oC$, for [2500 - 10000]:1:x resin formulations. For the sake of briefness, we refer the reader to Sects. S1 - S2 in the SI for a detailed description of the experimental methodology.

The numerical predictions in FROMP reactivity at $T_0 = 35^oC$, compared against the baseline case study with $T_0 = 23^oC$, are shown in Fig. 7 for an inhibitor loading equivalent of 0.5 (left) and 1.0 (right). For tabulated

numerical front velocities at both resin temperatures, we refer the reader to Tab. S4 and Tab. S5 in the SI.

Across both resin temperatures and inhibitor loading equivalents, we remark that the simulated polymerization front velocities are in good agreement with experiments, further validating the Occam's razor hypothesis. Moreover, in light of the temperature-dependent FROMP kinetics, front velocities increase with increase in the initial resin temperature.

Towards high-throughput efforts, we next demonstrate an application of our mechanism-based model to a different monomer/initiator/inhibitor resin system through construction of a "semi-inverse" problem for efficient integration between experiments and simulations to accelerate material discovery.

A "semi-inverse" workflow for closed-loop screening of frontally polymerized resins

We develop here a "semi-inverse" workflow for synergistic integration of experiments and computational models for closed-loop FROMP reactivity screening. A schematic illustration of the "semi-inverse" workflow is shown in Fig. 8(b), illustrating the bypass of infor-

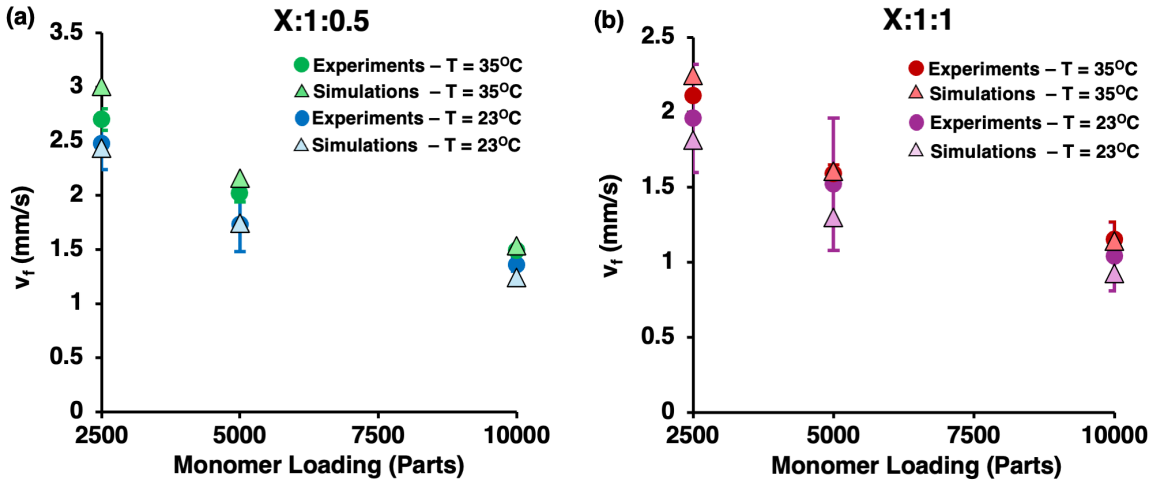

Figure 7: Variation in front velocity with change in the initial resin temperature for a DCPD:G2:TBP system with a monomer-to-initiator loading ratio of [2500-10000]:1 coupled to inhibitor molar equivalents of 0.5 (left) and 1.0 (right). Across the two different TBP inhibitor loadings (left to right), the simulated front velocities are shown to be in good quantitative agreement with the in-house experiments. All simulations use a consistent set of physiochemical parameters (Table 1).

mation between experiments and simulations. Upon selection of a monomer/initiator/inhibitor resin chemistry of interest, the transfer of information between experiments and the mechanism-based model is summarized below in a step-wise fashion:

(i) Step 1: Polymerization front velocity is experimentally measured at a single monomer:initiator:inhibitor composition for a resin chemistry of interest. The acquired experimental front velocity is subsequently passed to the mechanism-based model.

(ii) Step 2: Numerical simulations are performed with updated physiochemical parameters, reflective of the resin chemistry of interest, to obtain a polymerization front velocity consistent with the experimental data point provided.

(iii) Step 3: FROMP reactivity is numerically simulated for a series of monomer:initiator:inhibitor resin compositions of interest. Simulated front velocities are passed forward for experimental validation.

(iv) Step 4: FROMP reactivity is experimentally measured at the remaining monomer:initiator:inhibitor resin compositions of interest. Experimental front velocities are compared against numerical predictions for validation.

We remark here that apart from "Step 1", the remaining steps are performed in isolation from one another. That is, numerical FROMP reactivity predictions across the different resin compositions are performed first and separately from the experiments, the latter conducted only in "Step 4" for validation.

As a demonstration, we consider a distinct DCPD:M207:TBP resin chemistry, in which the Grubbs' 2nd generation initiator from the previous section is substituted with a M207 Grubbs' initiator by replacing the phenyl **Ph**-group in Fig. 3(b) with a 3-methyl-2-butenylidene constituent in Fig. 8(a).

Owing to the consistency of the mixture of phosphine/phosphite inhibitory ligands (i.e., PCy_3 and $P(OBu)_3$) and the N-heterocyclic carbene group, SIMes, $\Big($i.e., Fig. 8(a)$\Big)$, we assume the pre-initiation step remains unaltered and is described by the assumption of fast-equilibrium kinetics using the physiochemical parameters summarized in Tab. 1.

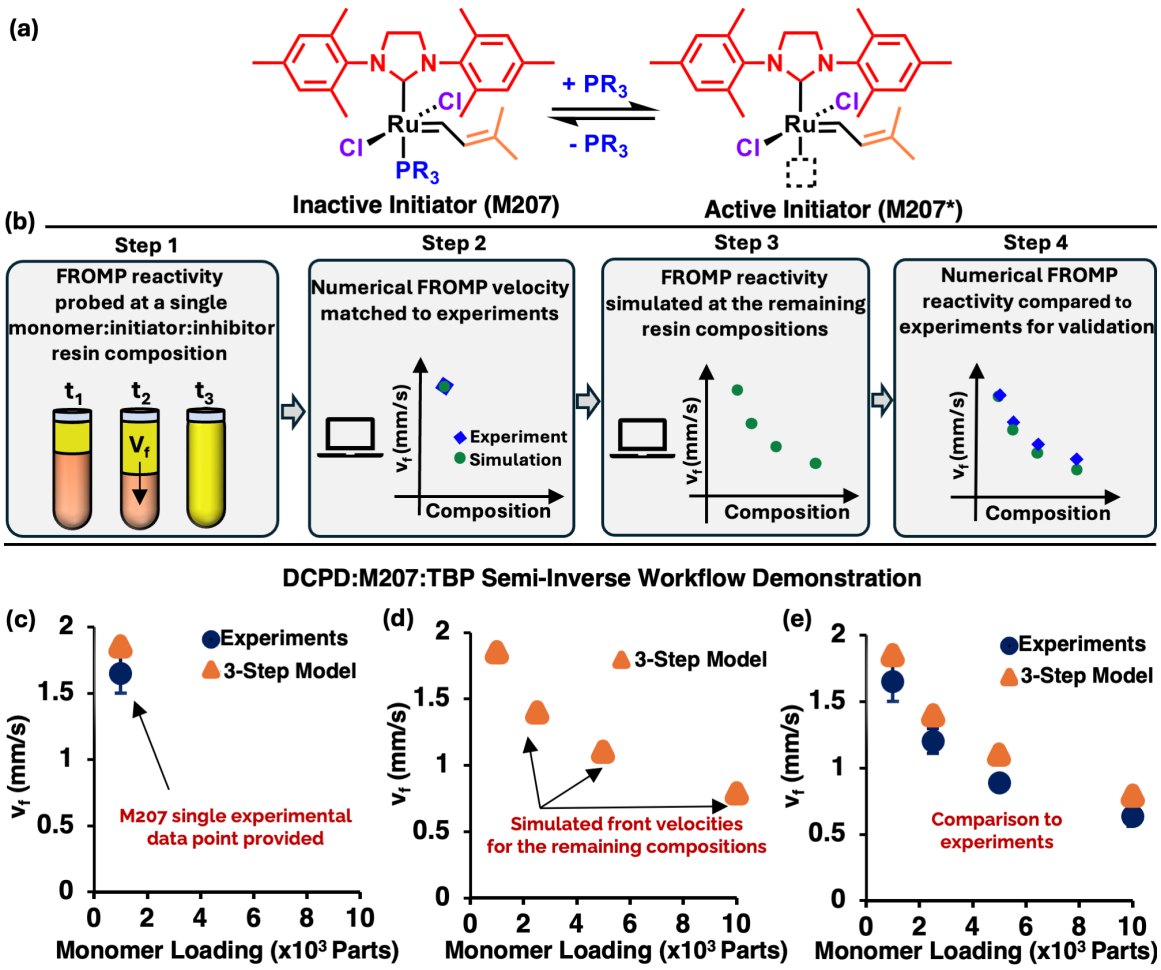

Figure 8: (a) Schematic illustration of the inhibitory ligand dissociation for a M207 Grubbs' initiator during the pre-initiation step. (b) Schematic illustration of the proposed semi-inverse workflow, showing the bypass of information between experiments and the mechanism-based computational model for accelerated FROMP reactivity screening across different resin compositions. (c – e) Demonstration of the semi-inverse workflow for probing FROMP reactivity in a DCPD:M207:TBP resin. Starting with a M207 single experimental data point, front velocities are numerically computed in isolation from experiments and shown to be in good quantitative agreement with the latter. See text for details on the selection of new physiochemical parameters.

This assumption is in line with the work of Sanford et al.[31] in which variations in the L-type and the PR_3 ligands (c.f. Fig. 2(a)) were demonstrated to have the most dominant effect on the pre-initiation step.

Nevertheless, variations in the electronic features of the 3-methyl-2-butenylidene R^1-substituent can modulate the affinity of the active ruthenium initiator to the DCPD monomer and as a result the initiation kinetics as

detailed below. Once the ruthenium-olefin complex has initiated, the subsequent irreversible chain growth polymerization proceeds in an identical manner as the previous Grubbs' 2$^{\text{nd}}$ generation initiated polydicyclopentadiene (pDCPD) formation. On this note, we preserve the propagation kinetic parameters for our DCPD:M207:TBP system to those reflected in Tab. 1. In light of the above discussion, the only necessary adjustable step for our DCPD:M207:TBP system is the initiation step. This requires a modulation in the effective initiation pre-exponential constant, A_i^{eff}.

To do so, FROMP reactivity is experimentally measured for a 1000:1:1 DCPD:M207:TBP resin composition. We refer the reader to Sects. S.1 – S.2 in the SI for a detailed description of the experimental methodology. Subsequently, the effective initiation pre-exponential constant, A_i^{eff}, is adjusted to obtain a numerical front velocity consistent with experiments $\Big($c.f. Fig. 8(c)$\Big)$. This yields $A_i^{eff} = 5.8 \cdot 10^9$ 1/s.

With the physiochemical properties modulated for our resin system at hand, polymerization front velocity is numerically simulated for a series of [1000–10000]:1:1 resin compositions $\Big($c.f. Fig. 8(d)$\Big)$. Subsequently, the simulated front velocities are passed forward to experimentalists. FROMP reactivity is experimentally measured at the remaining compositions and data collected is compared against the numerical front velocity predictions.

Fig. 8(e) illustrates the comparison between the experimental and the numerical front velocities for our DCPD:M207:TBP system. While the numerical and experimental data were collected in isolation, we observe that the simulated front velocities are in good quantitative agreement with the validation experiments. This not only further substantiates our Occam's razor hypothesis, but most importantly establishes – through the mechanism-based model – a closed loop integration between experiments and computational models for the efficient exploration of the vast chemical design space and the manufacturing of frontally-polymerized materials with enhanced engineering properties.

Conclusion

In this work, we formulate a novel chemically-grounded reaction-diffusion framework for frontally-polymerized thermosets. Presently, conventional models describing FROMP kinetics are phenomenological in nature, with cure kinetics parameters extracted from thermal analysis by DSC performed at different heating rates. Strict reliance on costly DSC measurements limits both (i) a chemically mechanistic understanding of the underlying FROMP reaction processes and (ii) the predictive capabilities of existing models on the role of variations in the resin composition on FROMP reactivity.

The proposed mechanism-based reaction-diffusion model addresses these limitations and systematically describes the reaction kinetics associated with each FROMP step, including pre-initiation which gates reactivity, initiation, and propagation. The ability of the model to reproduce FROMP reactivity with variation in the monomer:initiator:inhibitor loading for a DCPD:G2:TBP system at different processing conditions (i.e., initial resin temperature) was demonstrated in good agreement with experiments. Remarkably, we demonstrated that the ROMP mechanism and the associated physiochemical parameters are valid far from the conditions for which they were established, predicting FROMP macroscopic observables over a wide range of resin formulations.

Towards high-throughput efforts, a "semi-inverse" workflow for FROMP reactivity predictions in other monomer/initiator/inhibitor resin chemistries was additionally illustrated in an effort to efficiently integrate experiments and computational models for streamlined material screening.

In conclusion, the proposed framework presents a mechanism-based fast-screening computational tool which – in enabling for high-fidelity predictions of FROMP observables – can facilitate the identification of novel chemi–stries for the manufacturing of thermosets with superior thermo-chemo-mechanical properties.

Notes

The authors declare no financial competing interest.

Acknowledgement

This research was conducted in the Autonomous Materials Systems group at the Beckman Institute for Advanced Science and Technology at the University of Illinois Urbana-Champaign. The authors acknowledge support from the Department of Energy (Office of Basic Energy Sciences) as part of the Energy Frontier Research Center/Regenerative Energy-Efficient Manufacturing of Thermoset Polymeric Materials (REMAT) under award number DE-SC0023457. The authors additionally acknowledge Dr. Benjamin A. Suslick for the insightful chemistry discussions.

References

(1) Robertson, I. D.; Yourdkhani, M.; Centellas, P. J.; Aw, J. E.; Ivanoff, D. G.; Goli, E.; Lloyd, E. M.; Dean, L. M.; Sottos, N. R.; Geubelle, P. H.; others Rapid energy-efficient manufacturing of polymers and composites via frontal polymerization. *Nature* **2018**, *557*, 223–227.

(2) Suslick, B. A.; Hemmer, J.; Groce, B. R.; Stawiasz, K. J.; Geubelle, P. H.; Malucelli, G.; Mariani, A.; Moore, J. S.; Pojman, J. A.; Sottos, N. R. Frontal polymerizations: from chemical perspectives to macroscopic properties and applications. *Chemical reviews* **2023**, *123*, 3237–3298.

(3) Luo, T.; Ma, Y.; Cui, X. Review on Frontal Polymerization Behavior for Thermosetting Resins: Materials, Modeling and Application. *Polymers* **2024**, *16*, 185.

(4) Chekanov, Y. A.; Pojman, J. A. Preparation of functionally gradient materials via frontal polymerization. *Journal of Applied Polymer Science* **2000**, *78*, 2398–2404.

(5) Chen, S.; Sui, J.; Chen, L.; Pojman, J. A. Polyurethane–nanosilica hybrid nanocomposites synthesized by frontal polymerization. *Journal of Polymer Science Part A: Polymer Chemistry* **2005**, *43*, 1670–1680.

(6) Sanna, R.; Alzari, V.; Nuvoli, D.; Scognamillo, S.; Marceddu, S.; Mariani, A. Polymer hydrogels of 2-hydroxyethyl acrylate and acrylic acid obtained by

frontal polymerization. *Journal of Polymer Science Part A: Polymer Chemistry* **2012**, *50*, 1515–1520.

(7) Kim, C.; Teng, H.; Tucker, C. L.; White, S. R. The continuous cuing process for thermoset polymer composites. Part 1: modeling and demonstration. *Journal of Composite materials* **1995**, *29*, 1222–1253.

(8) Pojman, J. A.; Ilyashenko, V. M.; Khan, A. M. Free-radical frontal polymerization: Self-propagating thermal reaction waves. *Journal of the Chemical Society, Faraday Transactions* **1996**, *92*, 2825–2837.

(9) Goldfeder, P.; Volpert, V. A.; Ilyashenko, V.; Khan, A.; Pojman, J.; Solovyov, S. Mathematical modeling of free-radical polymerization fronts. *The Journal of Physical Chemistry B* **1997**, *101*, 3474–3482.

(10) McFarland, B.; Popwell, S.; Pojman, J. A. Free-radical frontal polymerization with a microencapsulated initiator: characterization of microcapsules and their effect on pot life, front velocity, and mechanical properties. *Macromolecules* **2006**, *39*, 55–63.

(11) Bomze, D.; Knaack, P.; Koch, T.; Jin, H.; Liska, R. Radical induced cationic frontal polymerization as a versatile tool for epoxy curing and composite production. *Journal of Polymer Science Part A: Polymer Chemistry* **2016**, *54*, 3751–3759.

(12) Scognamillo, S.; Bounds, C.; Thakuri, S.; Mariani, A.; Wu, Q.; Pojman, J. A. Frontal cationic curing of epoxy resins in the presence of defoaming or expanding compounds. *Journal of Applied Polymer Science* **2014**, *131*.

(13) Malik, M. S.; Schlögl, S.; Wolfahrt, M.; Sangermano, M. Review on UV-induced cationic frontal polymerization of epoxy monomers. *Polymers* **2020**, *12*, 2146.

(14) Alzari, V.; Nuvoli, D.; Sanna, D.; Ruiu, A.; Mariani, A. Effect of limonene on the frontal ring opening metathesis polymerization of dicyclopentadiene. *Journal of Polymer Science Part A: Polymer Chemistry* **2016**, *54*, 63–68.

(15) Robertson, I. D.; Pruitt, E. L.; Moore, J. S. Frontal ring-opening metathesis polymerization of exo-dicyclopentadiene for low catalyst loadings. *ACS Macro Letters* **2016**, *5*, 593–596.

(16) Kumar, A.; Gao, Y.; Geubelle, P. H. Analytical estimates of front velocity in the frontal polymerization of thermoset polymers and composites. *Journal of Polymer Science* **2021**, *59*, 1109–1118.

(17) Kumar, A.; Zakoworotny, M.; Bonner, F. J. B.; Aw, J. E.; Sottos, N. R.; Tawfick, S. H.; Geubelle, P. H. A thermo-chemo-mechanical model for material extrusion of frontally polymerizing thermoset polymers. *Additive Manufacturing* **2024**, *80*, 103972.

(18) Kumar, A.; Dean, L. M.; Yourdkhani, M.; Guo, A.; BenVau, C.; Sottos, N. R.; Geubelle, P. H. Surface pattern formation induced by oscillatory loading of frontally polymerized gels. *Journal of the Mechanics and Physics of Solids* **2022**, *168*, 105055.

(19) Goli, E.; Robertson, I. D.; Geubelle, P. H.; Moore, J. S. Frontal polymerization of dicyclopentadiene: a numerical study. *The Journal of Physical Chemistry B* **2018**, *122*, 4583–4591.

(20) Goli, E.; Gai, T.; Geubelle, P. Impact of boundary heat losses on frontal polymerization. *The Journal of Physical Chemistry B* **2020**, *124*, 6404–6411.

(21) Zakoworotny, M.; Bonner, F. J. B.; Kumar, A.; Aw, J. E.; Tawfick, S. H.; Ewoldt, R. H.; Sottos, N. R.; Geubelle, P. H. Rheological modeling of frontal-polymerization-based direct ink writing of thermoset polymers. *Computer Methods in Applied Mechanics and Engineering* **2024**, *418*, 116565.

(22) Li, X.; Cohen, T. Mechanical forces quench frontal polymerization: Experiments and theory. *Journal of the Mechanics and Physics of Solids* **2024**, *183*, 105517.

(23) Vyas, S.; Zhang, X.; Goli, E.; Geubelle, P. Frontal vs. bulk poly-

merization of fiber-reinforced polymer-matrix composites. *Composites Science and Technology* **2020**, *198*, 108303.

(24) Kessler, M. R.; White, S. R. Cure kinetics of the ring-opening metathesis polymerization of dicyclopentadiene. *Journal of Polymer Science Part A: Polymer Chemistry* **2002**, *40*, 2373–2383.

(25) Yang, G.; Lee, J. K. Curing kinetics and mechanical properties of endo-dicyclopentadiene synthesized using different Grubbs' catalysts. *Industrial & Engineering Chemistry Research* **2014**, *53*, 3001–3011.

(26) Jawiczuk, M.; Marczyk, A.; Trzaskowski, B. Decomposition of ruthenium olefin metathesis catalyst. *Catalysts* **2020**, *10*, 887.

(27) Hong, S. H.; Day, M. W.; Grubbs, R. H. Decomposition of a key intermediate in ruthenium-catalyzed olefin metathesis reactions. *Journal of the American Chemical Society* **2004**, *126*, 7414–7415.

(28) Neary, W. J.; Kennemur, J. G. Variable temperature ROMP: Leveraging low ring strain thermodynamics to achieve well-defined polypentenamers. *Macromolecules* **2017**, *50*, 4935–4941.

(29) Spade, C.; Volpert, V. On the steady-state approximation in thermal free radical frontal polymerization. *Chemical engineering science* **2000**, *55*, 641–654.

(30) Lessard, J. J.; Mejia, E. B.; Kim, A. J.; Zhang, Z.; Berkey, M. G.; Medina-Barreto, Z. S.; Ewoldt, R. H.; Sottos, N. R.; Moore, J. S. Unraveling Reactivity Differences: Room-Temperature Ring-Opening Metathesis Polymerization (ROMP) versus Frontal ROMP. *Journal of the American Chemical Society* **2024**,

(31) Sanford, M. S.; Love, J. A.; Grubbs, R. H. Mechanism and activity of ruthenium olefin metathesis catalysts. *Journal of the American Chemical Society* **2001**, *123*, 6543–6554.

(32) Cooper, J. C.; Paul, J. E.; Ramlawi, N.; Saengow, C.; Sharma, A.; Suslick, B. A.; Ewoldt, R. H.; Sottos, N. R.; Moore, J. S. Reprocessability in Engi-

neering Thermosets Achieved through Frontal Ring Opening Metathesis Polymerization. *Advanced Materials* **2024**, 2402627.

(33) Nason, C.; Roper, T.; Hoyle, C.; Pojman, J. A. UV-induced frontal polymerization of multifunctional (meth) acrylates. *Macromolecules* **2005**, *38*, 5506–5512.

(34) Frulloni, E.; Salinas, M.; Torre, L.; Mariani, A.; Kenny, J. M. Numerical modeling and experimental study of the frontal polymerization of the diglycidyl ether of bisphenol A/diethylenetriamine epoxy system. *Journal of applied polymer science* **2005**, *96*, 1756–1766.

(35) Trnka, T. M.; Morgan, J. P.; Sanford, M. S.; Wilhelm, T. E.; Scholl, M.; Choi, T.-L.; Ding, S.; Day, M. W.; Grubbs, R. H. Synthesis and activity of ruthenium alkylidene complexes coordinated with phosphine and N-heterocyclic carbene ligands. *Journal of the American Chemical Society* **2003**, *125*, 2546–2558.

(36) Mariani, A.; Fiori, S.; Chekanov, Y.; Pojman, J. A. Frontal ring-opening metathesis polymerization of dicyclopentadiene. *Macromolecules* **2001**, *34*, 6539–6541.

(37) Ruiu, A.; Sanna, D.; Alzari, V.; Nuvoli, D.; Mariani, A. Advances in the frontal ring opening metathesis polymerization of dicyclopentadiene. *Journal of Polymer Science Part A: Polymer Chemistry* **2014**, *52*, 2776–2780.

(38) Robertson, I. D.; Dean, L. M.; Rudebusch, G. E.; Sottos, N. R.; White, S. R.; Moore, J. S. Alkyl phosphite inhibitors for frontal ring-opening metathesis polymerization greatly increase pot life. *ACS Macro Letters* **2017**, *6*, 609–612.

(39) Scroggs, M. W.; Baratta, I. A.; Richardson, C. N.; Wells, G. N. Basix: a runtime finite element basis evaluation library. *Journal of Open Source Software* **2022**, *7*, 3982.

(40) Vyas, S.; Goli, E.; Zhang, X.; Geubelle, P. Manufacturing of unidirectional glass-fiber-reinforced composites via frontal polymerization: A numer-

ical study. *Composites Science and Technology* **2019**, *184*, 107832.

(41) Adlhart, C.; Chen, P. Mechanism and activity of ruthenium olefin metathesis catalysts: the role of ligands and substrates from a theoretical perspective. *Journal of the American Chemical Society* **2004**, *126*, 3496–3510.

TOC Graphic

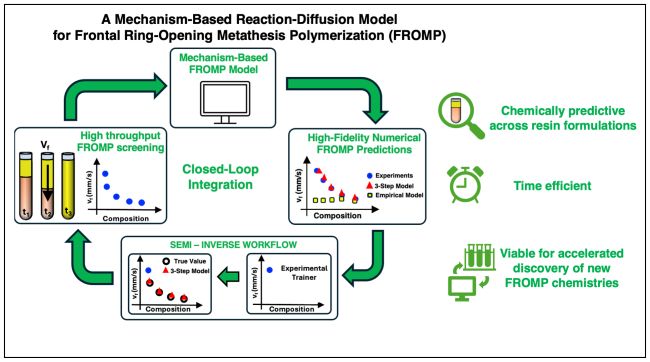

Supporting Information

We present here additional information pertinent to the following items:

1. Materials and Instrumentation
2. Experimental Procedures
3. Varied monomer:initiator:inhibitor loadings
4. Tabulated comparison of simulated versus experimental front speeds

Table of Contents

S.1 - Materials and Instrumentation

Materials

Dicyclopentadiene (DCPD, Cymetech ULTRENE™), ethylidene norbornene (ENB, MilliporeSigma), Grubbs' 2nd generation catalyst (G2, ChemScene), Grubbs' Catalyst M207 (M207, Sigma Aldrich), and tributyl phosphite (TBP, TCI chemicals) were purchased commercially and used as received unless otherwise stated.

Instrumentation

Samples weighing and sonication:

All masses were weighted using a Mettler Toledo precision balance with a ± 0.01 mg readability (see *"S.2 - Experimental Procedures"* for a detailed description). Sonication was performed using a Digital Ultrasonic bath to ensure adequate breakdown and proper mixing of catalyst particles in the resin prior to FROMP testing.

Resin Temperature and Velocity Measurements:

Frontal polymerization was video captured using a built-in iPhone camera. A custom-built Python software based on the OpenCV library was used to track the front location and calculate the average polymerization velocity. Resin samples tested at $T_0 = 35^{\circ}$C were heated inside a Thermo Scientific oven and their temperature measured using a T-type thermocouple interfacing with a custom Labview software prior to FROMP initiation.

S.2 - Experimental Procedures

General Procedure for Resin Preparation

Grubbs' 2nd generation or Grubbs' M207 initiator were massed (G2 or M207, **w** mg, 1.00 equivalent) in a 10 mL vial prior to addition of the tributyl phosphite inhibitor (TBP, **x** μL, **y** equivalent). The mixture was subsequently dissolved in a monomer solution (95:5 mol

DCPD:ENB, 2.00 g, **z** equiv.) and sonicated for three minutes. Values of {**w, x, y, z**} for the preparation of DCDP/ENB:M207:TBP resins are listed below. For values of {**w, x, y, z**} pertaining to the DCDP/ENB:G2:TBP resins, refer to Lessard et al.[1]

The resulting solution was transferred to a 10 mm-diameter test tube. Dependent on the experimental needs, test tubes were either maintained at room temperature or transferred inside a temperature-controlled oven for testing at an elevated starting resin temperature, $T_0 = 35^oC$. Frontal polymerization at the top of the resin solution was initiated using a preheated soldering iron, creating a descending front. Experiments were video recorded for data processing until the polymerization front reached the bottom of the test tube.

M207 Experiments:

10000:1:1 Monomer:Initiator:Inhibitor

M207: **w** = 1.26 mg

TBP: **x** = 0.4 μL; **y** = 1.0 equiv.

DCPD/ENB: **z** = 10000.0 equiv.

5000:1:1 Monomer:Initiator:Inhibitor

M207: **w** = 2.51 mg

TBP: **x** = 0.8 μL; **y** = 1.0 equiv.

DCPD/ENB: **z** = 5000.0 equiv.

2500:1:1 Monomer:Initiator:Inhibitor

M207: **w** = 5.03 mg

TBP: **x** = 1.6 μL; **y** = 1.0 equiv.

DCPD/ENB: **z** = 2500.0 equiv.

1000:1:1 Monomer:Initiator:Inhibitor

M207: **w** = 12.57 mg

TBP: **x** = 4.1 μL; **y** = 1.0 equiv.

DCPD/ENB: **z** = 1000.0 equiv.

S.3 - Varied monomer:initiator:inhibitor loadings

We present here tabulated concentration data associated with the different monomer:initiator:inhibitor compositions investigated in this work and serving as input to the mechanism-based model.

Table S 1: Monomer/Initiator/Inhibitor concentrations for resin compositions containing 0.25 TBP inhibitor equivalence with varied monomer loadings.

Monomer:Initiator:Inhibitor Loading	**[PR_3^0]** (mol/L)	**[II_0]** (mol/L)	**[M_0]**(mol/L)
10000:1:0.25	0.000185	0.00074	7.4
5000:1:0.25	0.00037	0.00148	7.4
2500:1:0.25	0.00074	0.00296	7.4
1000:1:0.25	0.00185	0.0074	7.4
500:1:0.25	0.0037	0.0148	7.4

Table S 2: Monomer/Initiator/Inhibitor concentrations for resin compositions containing 0.5 TBP inhibitor equivalence with varied monomer loadings.

Monomer:Initiator:Inhibitor Loading	**[PR_3^0]** (mol/L)	**[II_0]** (mol/L)	**[M_0]**(mol/L)
10000:1:0.5	0.00037	0.00074	7.4
5000:1:0.5	0.00074	0.00148	7.4
2500:1:0.5	0.00148	0.00296	7.4
1000:1:0.5	0.0037	0.0074	7.4
500:1:0.5	0.0074	0.0148	7.4

Table S 3: Monomer/Initiator/Inhibitor concentrations for resin compositions containing 1.0 inhibitor equivalence with varied monomer loadings.

Monomer:Initiator:Inhibitor Loading	**[PR_3^0]** (mol/L)	**[II_0]** (mol/L)	**[M_0]**(mol/L)
10000:1:1	0.00074	0.00074	7.4
5000:1:1	0.00148	0.00148	7.4
2500:1:1	0.00296	0.00296	7.4
1000:1:1	0.0074	0.0074	7.4
500:1:1	0.0148	0.0148	7.4

S.4 - Tabulated simulated versus experimental front speeds

We present here tabulated comparisons of simulated versus experimental front speeds across the different monomer:initiator:inhibitor resin compositions considered in this work.

Table S 4: Simulated polymerization front velocities for [500–10000]:1:x DCPD:G2:TPB resin compositions compared against the experiments by Lessard et al.[1]

Monomer:Initiator:Inhibitor Loading	V_f^{exp} (mm/s)	$Error_{exp}$ (mm/s)	V_f^{sim} (mm/s)
500:1:0.25	5.33	± 0.03	5.332
500:1:0.5	5.02	± 0.21	4.991
500:1:1	3.68	± 0.16	3.719
1000:1:0.25	4.18	± 0.04	3.964
1000:1:0.5	3.29	± 0.25	3.718
1000:1:1	2.48	± 0.18	2.772
2500:1:0.25	2.49	± 0.58	2.598
2500:1:0.5	2.48	± 0.24	2.437
2500:1:1	1.96	± 0.36	1.816
5000:1:0.25	1.91	± 0.18	1.861
5000:1:0.5	1.73	± 0.25	1.745
5000:1:1	1.52	± 0.44	1.299
10000:1:0.25	1.54	± 0.09	1.323
10000:1:0.5	1.36	± 0.06	1.240
10000:1:1	1.04	± 0.23	0.924

*Experimental data by Lessard et al.[1] reported for a room-temperature, $T_0 = 23^oC$, liquid resin.

Table S 5: Simulated versus experimental polymerization front velocities for [2500–10000]:1:x DCPD:G2:TBP resin compositions at an elevated initial resin temperature, $T_0 = 35°C$.

Monomer:Initiator:Inhibitor Loading	V_f^{exp} (mm/s)	$Error_{exp}$ (mm/s)	V_f^{sim} (mm/s)
2500:1:0.5	2.7	± 0.10	3.013
5000:1:0.5	2.02	± 0.08	2.158
10000:1:0.5	1.49	± 0.03	1.535
2500:1:1	2.11	± 0.03	2.245
5000:1:1	1.59	± 0.06	1.607
10000:1:1	1.15	± 0.12	1.142

Table S 6: Simulated versus experimental polymerization front velocities for [1000–10000]:1:1 DCPD:M207:TBP resin compositions.

Monomer:Initiator:Inhibitor Loading	V_f^{exp} (mm/s)	$Error_{exp}$ (mm/s)	V_f^{sim} (mm/s)
1000:1:0.5	1.65	± 0.15	1.852
2500:1:0.5	1.203	± 0.093	1.398
5000:1:0.5	0.89	± 0.05	1.099
10000:1:0.5	0.64	± 0.07	0.790

References

(1) Lessard, J. J.; Mejia, E. B.; Kim, A. J.; Zhang, Z.; Berkey, M. G.; Medina-Barreto, Z. S.; Ewoldt, R. H.; Sottos, N. R.; Moore, J. S. Unraveling Reactivity Differences: Room-Temperature Ring-Opening Metathesis Polymerization (ROMP) versus Frontal ROMP. *Journal of the American Chemical Society* **2024**, *146*, 7216–7221.